Use of multiple LIDAR-derived digital terrain indices and machine learning for high-resolution national-scale soil moisture mapping of the Swedish forest landscape

Anneli M. Ågren [*], Johannes Larson, Siddhartho Shekhar Paul, Hjalmar Laudon, William Lidberg

Department of Forest Ecology and Management, Swedish University of Agricultural Science, Umeå, Sweden

ABSTRACT

Spatially extensive high-resolution soil moisture mapping is valuable in practical forestry and land management, but challenging. Here we present a novel technique involving use of LIDAR-derived terrain indices and machine learning (ML) algorithms capable of accurately modeling soil moisture at 2 m spatial resolution across the entire Swedish forest landscape. We used field data from about 20,000 sites across Sweden to train and evaluate multiple ML models. The predictor features (variables) included a suite of terrain indices generated from a national LIDAR digital elevation model and ancillary environmental features, including surficial geology, climate and land use, enabling adjustment of soil moisture class maps to regional or local conditions. Extreme gradient boosting (XGBoost) provided better performance for a 2-class model, manifested by Cohen's Kappa and Matthews Correlation Coefficient (MCC) values of 0.69 and 0.68, respectively, than the other tested ML methods: Artificial Neural Network, Random Forest, Support Vector Machine, and Naïve Bayes classification. The depth to water index, topographic wetness index, and 'wetland' categorization derived from Swedish property maps were the most important predictors for all models. The presented technique enabled generation of a 3-class model with Cohen's Kappa and MCC values of 0.58. In addition to the classified moisture maps, we investigated the technique's potential for producing continuous soil moisture maps. We argue that the probability of a pixel being classified as wet from a 2-class model can be used as a 0–100% index (dry to wet) of soil moisture, and the resulting maps could provide more valuable information for practical forest management than classified maps.

1. Introduction

Soil moisture plays crucial roles in terrestrial ecosystem processes, including energy, water, and carbon cycles (Seneviratne et al., 2010). Thus, spatially explicit assessment of soil moisture is essential for understanding energy and water budgets at scales ranging from local to global (Ali et al., 2015). Remote sensors of various kinds (e.g., passive, active or thermal) are mainly used for spatially extensive soil moisture mapping now (Mohanty et al., 2017; Zeng et al., 2019). Soil moisture maps derived from previous generations of satellite remote sensing systems generally have much too low spatial resolution for practical purposes (Mohanty et al., 2017), even with the use of algorithms that can enhance resolution to 500–1000 m (Bauer-Marschallingere et al., 2019; Sabaghy et al., 2020; Zeng et al., 2019). However, the European earth observation program Copernicus is providing radar and optical satellite data at higher (~10 m) resolution from the Sentinel mission.

Moreover, recent integrations of Sentinel-1 and Sentinel-2 datasets have yielded landscape-scale soil moisture maps of several regions with 10–100 m spatial resolution (El Hajj et al., 2017; Gao et al., 2017). Satellite data can also provide valuable temporal information, but even such high-resolution Sentinel data may not provide sufficient information for many small-scale land use management purposes, such as assessment of soil's bearing capacities to avoid damaging its structure during forestry and agricultural operations (Edwards et al., 2016). Thus, there are clear needs for alternative methods that can provide accurate soil moisture maps with high spatial resolution.

For smaller areas, field observations can be utilized to produce high-quality soil moisture maps, but such an approach is highly laborious and costly for regional-scale mapping. An established method to map soil moisture in more detail is to model hydrological features from digital elevation models (DEMs) (Akumu et al., 2019; Lidberg et al., 2020; Tenenbaum et al., 2006). Modeling soil moisture from DEMs rather than

using satellite remote sensing methods is especially suitable in forested ecosystems where the tree canopy obscures the soils (Lidberg et al., 2020). Following development of the topographic wetness index (TWI) by (Beven and Kirkby, 1979), several digital terrain indices have been introduced that can provide indications of soil moisture levels, such as the depth-to-water (DTW) index (Murphy et al., 2008), elevation above stream (EAS) index (Rennó et al., 2008) and downslope index (DI) (Hjerdt et al., 2004). Further, the DEMs' resolution has increased from 50 to 100 m two decades ago to a few meters, and even 0.5 m recently (Leempoel et al., 2015) with use of air-borne Light Detection and Ranging (LIDAR) measurements. Hence, soil moisture can now be modeled much more precisely, allowing more correct identification of smaller landscape elements. However, there has been little exploration of the possibilities offered by using a suite of terrain indices derived from high-resolution LIDAR data for high-resolution mapping of soil moisture over large landscapes.

One of the most commonly applied topographical indices in maps used in practical land management is the DTW (Murphy et al., 2007). Maps based on this index are used for planning forest management in several northern boreal countries, such as Canada and Sweden, and have recently been released for Finland. They often show previously unmapped stream networks and associated wet soils, thereby enabling more 'surprise-free' operational forest management planning (Murphy et al., 2008). However, there are two key requirements for generating DTW maps. One is selection of an appropriate threshold for flow initiation (the surface area needed for sufficient accumulation of water for transition from groundwater to surface water). A major complication is that this threshold varies substantially at both local and regional scales depending on soil transmissivity, topography, and weather conditions (Jaeger et al., 2019; Jensen et al., 2017). The other is to identify areas with wet soils using the DTW index. For this, a DTW threshold of 1 m is commonly used (Murphy et al., 2011; Ågren et al., 2014b), but the threshold should also be adjusted to local conditions to produce more accurate maps. Information on local conditions, including variation in soil transmissivity, topography, and local weather is crucial for accurate soil moisture mapping.

High-resolution (~2 m) terrain indices derived from airborne LIDAR imaging can accurately capture fine-scale landscape variations for predicting soil moisture, but integrating LIDAR indices over a large landscape can become extremely data-intensive. However, machine learning (ML) provides an effective approach for analyzing large-scale, heterogeneous datasets. For example, Lidberg et al. (2020) used ML models for mapping soil moisture class by combining information from LIDAR-derived, high-resolution (2 m) topographic indices calculated at different scales with various thresholds. Four types of ML models (Artificial Neural Network, Random Forest, Support Vector Machine, and Naïve Bayes classification) were trained and tested, using classified field soil moisture from the Swedish National Forest Inventory (hereafter NFI) to produce soil moisture class maps. The results demonstrated the potential utility of the approach, but so far efforts to map soil moisture using digital terrain indices have mostly focused on locating soils at the wet end of the spectrum, as wet soils are most sensitive to rut formation during forestry operations (Lidberg et al., 2020; White et al., 2012; Ågren et al., 2014b). Thus, areas in the final map generated by (Lidberg et al., 2020) were divided into only two classes: 'wet' areas where use of heavy machinery should be avoided or soils protected during off-road driving, and 'dry' areas with less sensitivity to soil disturbance.

Maps showing more classes of soil moisture across the gradient from dry to wet would be valuable for both the research community and forest practitioners, for several reasons. *Inter alia*, soil's bearing capacity largely depends on its moisture content (Ågren et al., 2014b), and multiclass or continuous soil moisture maps would be useful for diverse purposes such as optimizing tree production (Wei et al., 2018), road systems, off-road routes, riparian protection zones, ditches and other water management features (Erdozain et al., 2020; Kuglerová et al.,

2014a). Integration of LIDAR-derived terrain indices using multiple ML models for multi-class and continuous soil moisture mapping has substantial potential utility for such practical land management, but has received little attention to date. Incorporating ancillary spatial information regarding surficial geology, soil, hydrology, and land use could also enhance soil moisture models' predictions. Thus, in the study reported here we applied a suite of LIDAR-derived high-resolution terrain indices, auxiliary environmental variables, and several ML algorithms to generate 2-, 3- and 5-class soil moisture maps of the entire Swedish forest landscape. The algorithms included the relatively new Extreme Gradient Boosting (XGBoost) presented by Chen and Guestrin, (2016), which to the best of our knowledge has not been previously applied for regional-scale soil moisture classification and mapping. Soil moisture varies seasonally depending on weather conditions, but our modeling focused on the spatial distribution of average soil moisture levels. Thus, the overall aims were to generate and evaluate national-scale predictions of soil moisture, covering the whole range from dry to wet soils, using information with high spatial resolution on key environmental variables and multiple ML algorithms. We addressed the following specific questions. In combination with data on related environmental variables, can LIDAR-derived high-resolution terrain indices provide accurate multi-class and continuous soil moisture maps covering the entire Swedish forest landscape? Which ML algorithm provides the best predictions? Is there any location-specific variability in model performance across the study region?

2. Material and methods

The study involved analysis of data acquired from airborne LIDAR remote sensing, information on the NFI field plots, digital terrain indices, and ancillary environmental (pedological, geological, land use, and climatic) information. The data were integrated using several ML algorithms for soil moisture predictions (Fig. 1).
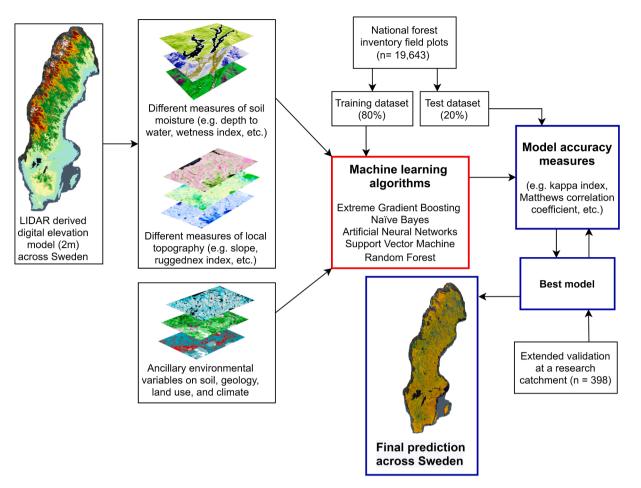
2.1. Full study site – The Swedish forest landscape

Sweden (latitude 55-70° N, longitude 11-25° E) is situated in Northern Europe, largely within the boreal zone (Fig. 2). Quaternary deposits dominated by glacial till cover most (75%) of the surface, and peat 13% of Sweden. Forest, agricultural land, heathlands, open mire, rock outcrops and urban areas respectively account for 69, 8, 8, 7, 5 and 3% of the national land cover, excluding the ca. 9% (4 million ha) of surface waters (Schöllin and Daher, 2019). Annual precipitation in Sweden ranges from 400 to 2100 mm (1961–1990), with the mountainous western region and southwestern parts receiving more precipitation than eastern parts, according to Swedish Metrological and Hydrological Institute web maps.

2.2. Field data – Swedish national forest Inventory

The new multiclass ML models were trained using data pertaining to 19,643 field plots monitored in the Swedish NFI (Fridman et al., 2014), which have a spatial accuracy of 5–10 m. The NFI compiles data on both productive forest land (defined as areas with a potential yield capacity of > 1 m^3 mean annual increment per ha) and low-productivity forestland (with lower yield capacity), such as pastures, thin soils, peatlands, rock outcrops, and areas close to and above the tree line. Areas outside forest land, such as crop fields, urban areas, roads, rail roads and power lines are not included in the NFI's sampling. Hence, the training dataset covered the soil moisture spectra in areas with all types of forest cover in Sweden (Fig. 2).

Soil moisture classes registered in the NFI , are based on each plot's average ground water level (estimated from its position in the landscape) and vegetation patterns. This approach reduces discrepancies caused by seasonal variation and provides indications of the general wetness regime, which is the key concern here. The NFI field plots are

Fig. 1. Schematic diagram showing the steps applied to produce a soil moisture map covering the entire Swedish forest landscape. Several measures of soil moisture and local topography were calculated from a high-resolution LiDAR-derived digital elevation model (2 × 2 m resolution). The map was regionally adjusted by including ancillary data on soils, climate etc. In total, maps of 28 features were used as inputs for the ML models, which were trained on soil moisture classes from 80% of the NFI field plots. Several ML algorithms were evaluated, and the resulting models' accuracy was evaluated by using the other 20% of the NFI plots as a test set and the best model was iteratively derived. We also evaluated the best model for a specific research catchment. The best ML model was applied to maps covering all of Sweden to predict soil moisture across the entire country.

categorized in five classes—mesic (the most common class), followed by mesic-moist, moist, dry and wet (Fig. 3)—which are described below and presented in more detail by (Fridman et al., 2014; Lidberg et al., 2020).

Wet Soils - Wet soils are normally located in open peatlands classified as bogs or fens, where trees may occasionally occur but not in dense stands. The groundwater table is close to the soil surface and permanent ponds are common. The soils are histosols or gleysols. The organic layer is often > 30 cm thick. Feet will be soaked when walking on wet soils in shoes, and it is often impossible for heavy machinery to cross them unless they are frozen during winter.

Moist soils - Moist soils are in areas with shallow groundwater (<1 m). Pools of standing water are visible in local pits. These areas can be crossed dry-footed in shoes if relatively high parts and tussocks are used, but a pool of water will form around the shoes in lower-lying areas, even after dry spells. The soils are histosols, gleysols, or regosols (weakly developed mineral soils that cannot be classified in any of the other World Reference Base reference groups). Vegetation is dominated by wetland mosses (e.g. *Sphagnum* spp., *Polytrichum commune, Polytrichastrum formosum, Polytrichastrum longisetum*) and *Sphagnum* spp. dominate local depressions. Trees have coarse root systems above ground and tussocks are common, indicating adaptation to high groundwater levels in these areas. The thickness of the organic layer is not used to define moist areas, but it is often > 30 cm.
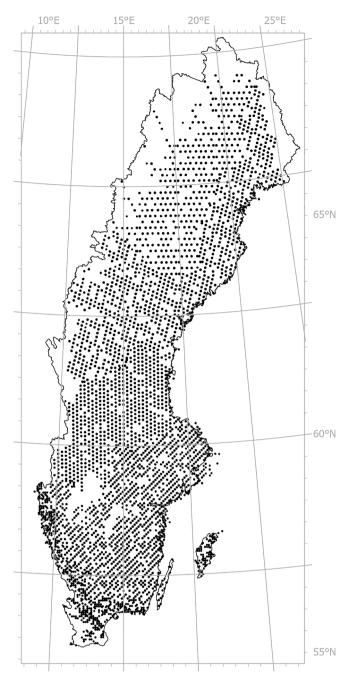
Mesic-moist soils – These soils are in areas where the groundwater

table is < 1 m from the surface, normally with flat or low-lying ground, or on lower parts of hills. They become wet seasonally following snowmelt or rain, and the possibility to cross them dry-footed depends on the season. Wetland mosses (e.g. *Sphagnum* spp., *Polytrichum commune, Polytrichastrum formosum, Polytrichastrum longisetum*) are common and trees have coarse root systems above ground, indicating that groundwater levels are often high in these areas. Soils are humo-ferric to humus-podzols. The organic layer is thicker than in mesic soils, and while podzols are common the O-horizon is still often peaty.

Mesic soils - Mesic soils consist of ferric podzols with a thin humus layer covered mainly by dryland mosses (e.g. *Pleurozium schreberi, Hylocomium splendens, Dicranum scoparium*). The groundwater table is 1–2 m below the soil surface generally. They can be walked on dry-footed even directly after rain or shortly after snowmelt. The organic layers are normally 4–10 cm thick.

Dry soils – In these soils the groundwater table is at least 2 m below the surface. They tend to be coarse-textured and can be found on hills, eskers, ridges and marked crowns. The soils are podzols (which have thin organic and bleached horizons), leptosols, arenosols, or regosols.

The soil moisture classes were grouped to generate ML models with five, three or two classes, as shown in Table 1. The 5-class models were trained using each of the five NFI soil moisture classes. In the 3-class models, as there were relatively few observations of the most extreme classes (dry and wet) they were grouped with their neighboring classes. In the 2-class models the five classes were merged into two classes,

Fig. 2. Locations of the 19 643 NFI field plots (black points). The density of field plots is higher in southern Sweden than in northern Sweden and the white regions in northwestern Sweden had not been scanned with LIDAR at the time of this study or indicate areas above the tree line. White parts in southern Sweden are large lakes or agricultural land.

simply called 'dry' and 'wet', following terminology used by Lidberg et al. (2020).

2.3. Collating input features to the model

In accordance with the context and approach of the study, we use the term features (from machine learning terminology), variables or measures (from general research terminology) or indices (from GIS terminology) to denote inputs of the ML models. Geospatial data from several sources were combined to train the ML models to predict soil moisture classes (Table 2). First, we extracted a set of digital terrain indices from the Swedish National DEM generated from a 0.5–1 points per m² LIDAR
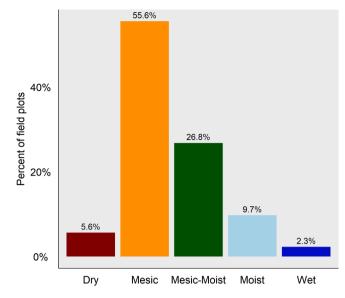

Fig. 3. Percentages of field plots in the soil moisture categories of the National Forest Inventory dataset (n = 19,643).

Table 1
Grouping of the NFI soil moisture data used in the 5-, 3- and 2-class models.

5-class models	3-class models	2-class models
Dry	Dry-mesic	'Dry'
Mesic		
Mesic-moist	Mesic-moist	'Wet'
Moist	Moist-wet	
Wet		

cloud by the Swedish Mapping, Cadastral and Land Registration Authority. This DEM has 2 m spatial resolution and input features derived from it were described in detail by Lidberg et al. (2020). The measures of local topography were calculated from the raw DEM while the soil moisture measures (Table 2) were calculated from a DEM processed by burning streams from the topographic maps across roads (Lidberg et al., 2017) and applying breaching as explained by (Lindsay, 2016). The soil moisture and local topography measures were all calculated from the 2 m national DEM, apart from the Topographic Wetness Index (TWI), which has been found to give unrealistic results when calculated at high resolution (Sørensen and Seibert, 2007; Ågren et al., 2014b). Therefore, TWI was calculated at coarser resolutions (10–48 m) deemed sufficient to capture the macro-topographical control of hydrological pathways. By including different window sizes (6 × 6 m to 160 × 160 m) we evaluated both macro- and micro-topographic effects on these pathways (Table 2). However, as we were applying substantially higher resolution than many other studies, it also enabled us to evaluate the modeling utility of more 'small-scale features'. For this purpose we incorporated the following digital terrain indices in addition to those described by (Lidberg et al., 2020)—the downslope index (Hjerdt et al., 2004), standard deviation of mean elevation within a moving window of 7 × 7 DEM cells, standard deviation from slope with a moving window of 3 × 3 cells, circular variance of aspect with a 3 × 3 moving window, and ruggedness index—all calculated from the 2 m DEM. For an explanation of these indices see the WhiteboxTools User Manual (Lindsay, 2020). By including more of these 'small-scale features' we aimed to improve the modelling of soil moisture in local pits and small-scale variability in riparian zones. Ancillary environmental variables used to capture variability in climatic and soil conditions were: quaternary deposits and soil depth from the Swedish Geological Survey; wetlands from the Swedish Mapping, Cadastral and Land Registration Authority; runoff from the Swedish Metrological and Hydrological Institute; and land-use from the

Table 2

Input variables used to model soil moisture classes, including digital terrain indices and ancillary environmental variables, calculated as described by [1](Lidberg et al., 2020) and [2](Lindsay, 2020). Abbreviations refer to the designations in Fig. 4. Features included in the final model are marked in black and features that were evaluated but excluded from the final model are marked in grey.

In-data map layers used to classify soil moisture	Utilized scales, thresholds and seasons	Data source	Short name
Soil moisture measures			
Depth to water 0.5 ha [1]	Stream initiation threshold 0.5 ha	Calculated from the 2 m DEM	DTW 0.5 ha
Depth to water 1 ha [1]	Stream initiation threshold 1 ha	Calculated from the 2 m DEM	DTW 1 ha
Depth to water 2 ha [1]	Stream initiation threshold 2 ha	Calculated from the 2 m DEM	DTW 2 ha
Depth to water 5 ha [1]	Stream initiation threshold 5 ha	Calculated from the 2 m DEM	DTW 5 ha
Depth to water 10 ha [1]	Stream initiation threshold 10 ha	Calculated from the 2 m DEM	DTW 10 ha
Depth to water 15 ha [1]	Stream initiation threshold 15 ha	Calculated from the 2 m DEM	DTW 15 ha
Depth to water 30 ha [1]	Stream initiation threshold 30 ha	Calculated from the 2 m DEM	DTW 30 ha
Down slope index [2]	2 m drop threshold	Calculated from the 2 m DEM	DI 2 m
Topographic wetness index [1]	10 m × 10 m	Calculated from a 10 m DEM resampled to 2 m	TWI 10 m
Topographic wetness index [1]	24 m × 24 m	Calculated from a 24 m DEM resampled to 2 m	TWI 24 m
Topographic wetness index [1]	48 m × 48 m	Calculated from a 48 m DEM resampled to 2 m	TWI 48 m
Elevation above stream 0.5 ha [1]	Stream initiation threshold 0.5 ha	Calculated from the 2 m DEM	EAS 0.5 ha
Elevation above stream 1 ha [1]	Stream initiation threshold 1 ha	Calculated from the 2 m DEM	EAS 1 ha
Elevation above stream 2 ha [1]	Stream initiation threshold 2 ha	Calculated from the 2 m DEM	EAS 2 ha
Elevation above stream 5 ha [1]	Stream initiation threshold 5 ha	Calculated from the 2 m DEM	EAS 5 ha
Elevation above stream 10 ha [1]	Stream initiation threshold 10 ha	Calculated from the 2 m DEM	EAS 10 ha
Elevation above stream 15 ha [1]	Stream initiation threshold 15 ha	Calculated from the 2 m DEM	EAS 15 ha
Elevation above stream 30 ha [1]	Stream initiation threshold 30 ha	Calculated from the 2 m DEM	EAS 30 ha
Local topography measures			
Elevation [1]	Elevation of each field plot	Calculated from the 2 m DEM	Elevation
Standard deviation from mean elevation [2]	Standard deviation from mean elevation	Calculated from the 2 m DEM	DFME

Table 2 (*continued*)

	with a 7 x 7 cell moving window		
Standard deviation from elevation [1]	Standard deviation from the digital elevation model with a 5 x 5 cell moving window	Calculated from the 2 m DEM	STDV 5 Cells
Standard deviation from elevation [1]	Standard deviation from the digital elevation model with a 10 x 10 cell moving window	Calculated from the 2 m DEM	STDV 10 Cells
Standard deviation from elevation [1]	Standard deviation from the digital elevation model with a 20 x 20 cell moving window	Calculated from the 2 m DEM	STDV 20 Cells
Standard deviation from elevation [1]	Standard deviation from the digital elevation model with a 40 x 40 cell moving window	Calculated from the 2 m DEM	STDV 40 Cells
Standard deviation from elevation [1]	Standard deviation from the digital elevation model with a 80 x 80 cell moving window	Calculated from the 2 m DEM	STDV 80 Cells
Standard deviation from slope [2]	Standard deviation from slope with a 3 x 3 cell moving window	Calculated from the 2 m DEM	SDFS
Circular variance of aspect [2]	Circular variance of aspect with a 3 x 3 cell moving window	Calculated from the 2 m DEM	CVA
Ruggedness [2]	Ruggedness index	Calculated from the 2 m DEM	Ruggedness
Slope [2]	Slope	Calculated from the 2 m DEM	Slope
Ancillary environmental variables			
Quaternary deposits - Peat Soil [1]	Extracted from the best map available at each	Digital map from the Geological Survey of Sweden	Peat Soil

Table 2 (*continued*)

	field plot (with scales differing among regions)		
Quaternary deposits – Glacial till [1]	-||-	-||-	Till soil
Quaternary deposits - Fine sediment [1]	-||-	-||-	Fine sediment
Quaternary deposits – Coarse Sediment [1]	-||-	-||-	Coarse sediment
Quaternary deposits - Thin soil [1]	-||-	-||-	Thin soil
Soil depth	Modelled soil depth	-||-	Soil depth
Wetlands from the Swedish property map [1]	1:12 500 scale	From the Swedish Mapping, Cadastral and Land Registration Authority	Wetlands
Winter Runoff [1]	30-year average winter runoff	Digital map from Swedish Metrological and Hydrological Institute, Calculated with S-HYPE	Winter Runoff
Summer Runoff [1]	30-year average summer runoff	-||-	Summer Runoff
Autumn Runoff [1]	30-year average autumn runoff	-||-	Autumn Runoff
Annual Runoff [1]	30-year average annual runoff	-||-	Annual Runoff
Spring Runoff [1]	30-year average spring runoff	-||-	Spring Runoff
X Coordinates of field plots [1]	X coordinates in SWEREFF 99 TM	NFI	X Coordinate
Y Coordinates of field plots [1]	Y coordinates in SWEREFF 99 TM	NFI	Y Coordinate
National land use data	10 m x 10 m	Swedish Environmental Protection Agency	CORINE
Soil moisture index	10 m x 10 m	Swedish Environmental Protection Agency	SMI

national land cover database as well as a 10 m resolution soil moisture index from the Swedish Environmental Protection Agency (SEPA). These data, summarized in Table 2, were resampled to 2 m grids to match the LIDAR-derived variables.

2.4. Evaluation of ML algorithms

We evaluated five ML algorithms commonly used for environmental modeling and remote sensing-based prediction—Extreme Gradient Boosting (Chen et al., 2020), Naïve Bayes (Bhargavi and Jyothi, 2009), Artificial Neural Networks (Ripley, 1996), Support Vector Machine (Chang and Lin, 2011), and Random Forest (Breiman, 2001). The calculations were performed in R (R Core Team, 2020) using the software packages Caret 6.0–86 (Kuhn et al., 2012) and XGBoost 1.0.0.2 (Chen et al., 2020). In the following text, ML algorithms and ML models respectively refer to the algorithms *per se*, and the 2-, 3- and 5-clas models generated with them (Table 1). The NFI field plots were divided randomly into a training set and test set, respectively, including 80 and 20% of the plots. Data pertaining to these sets were respectively used to train the ML algorithms, with default tuning parameters, and evaluate the final models. A 2.5 km × 2.5 km area was used to evaluate the processing time required for each ML algorithm to generate a predicted soil moisture map. The ML algorithms were evaluated using Cohen's Kappa Coefficient (Cohen, 1960), hereafter Kappa, and Matthews Correlation Coefficient (MCC) (Matthews, 1975), as well as the time required to acquire the predictions.

2.5. Feature reduction

In total, 44 features were evaluated as predictors for soil moisture in the ML models (Table 2). To avoid overparameterization, feature reduction is an integral part of any complex ML approach, and we applied three criteria for discarding the least influential variables: high correlation with other variables, minor contribution to the models based on variable importance scores, and manifestation in the predicted maps of inaccuracies related to overfitting or other unrealistic outcomes (Maxwell et al., 2018). The following features were removed. First, elevation above stream (Rennó et al., 2008), with all thresholds, was excluded because it showed similar patterns to DTW, but with lower accuracy. Depth-to-water (DTW) 10 and 15 ha, annual runoff, spring runoff, standard deviation from elevation with moving windows>5 × 5 cells and 10 m × 10 m land use map (CORINE) were evaluated but excluded due to low contribution to the models or multicollinearity. The 10 m × 10 m soil moisture index (SMI) from SEPA ranked high among predictor variables, but produced unrealistic outcomes (large pixels) on the maps and hence was excluded. Excluding SMI did not affect the overall performance of the models, possibly because TWI 10 m, DTW, and quaternary deposits (input data for the SMI) were included separately among the 28 features. After the feature reduction step, 28 features were included in the final predictive model.

2.6. Calibration and validation of the ML models

We concluded from the algorithm appraisal that XGBoost was the best ML algorithm (Table 3), so the rest of the article focuses on the analysis using it. XGBoost is a decision-tree-based ensemble algorithm that applies a gradient boosting framework. Gradient boosting is used to minimize errors by a gradient descent algorithm. XGBoost improves on this by using regularized gradient boosting. Great efforts have also been made to optimize parallelization and hardware to improve its computational performance. XGBoost (Chen and Guestrin, 2016) was applied with a dropout technique (gbDART), in which random trees are dropped to reduce overfitting (Rashmi and Gilad-Bachrach, 2015).

The training dataset consisted of estimates of soil moisture class in the NFI field plots classified using the selected number of soil moisture classes (Table 1) and features (Table 2). For XGboost we applied more

Table 3

Performance of the tested ML algorithms for predicting soil moisture class in terms of Cohen's Kappa Coefficient (Kappa) and Matthews Correlation Coefficient (MCC), calculated using the test dataset (pertaining to 20% of the NFI plots). Prediction time refers to the time required for applying the tuned model to one 2.5 × 2.5 km^2 raster tile.

Algorithm	Kappa	MCC	Prediction time
Extreme Gradient Boosting	0.68	0.68	1.1 min
Naïve Bayes	0.61	0.61	1.2 min
Artificial Neural Network	0.66	0.67	1.4 min
Support Vector Machine	0.67	0.67	5.1 min
Random Forest	0.66	0.66	2.0 min

extensive tuning for the 2-, 3- and 5-class models. The optimal hyperparameters from the tuning process were selected by an iterative tuning approach (with 10-fold cross-validation using Kappa as a metric (SI 1–3)). The final models were trained using the training dataset and tested using the test dataset (pertaining to 80% and 20% of the NFI field plots, respectively). The input features were split into 73 000 multiband raster tiles with 2.5 km × 2.5 km size and 2 m × 2 m resolution. This enabled multiple tiles to be predicted in parallel, dramatically reducing the required processing time. Even so, it took five days to predict soil moisture for all of the Swedish forest landscape using a 32-core (64-thread) processor running at 3.2 GHz. To spread this methodology we publish the entire R code (with explanations) for the three XGBoost models (SI 1–3).

2.7. Evaluating the XGBoost models using 20% of the NFI plots

The accuracy of the classified models was investigated using several measures (Table 4): overall accuracy (Story and Congalton, 1986), Kappa, MCC, recall (also known as sensitivity) and F1-values (the harmonic mean of sensitivity and precision) (Powers, 2011) and others, including confusion matrixes, described in the supporting information. The measures were calculated in R 4.0 using Caret 6.0–86 and Yardstick 0.07. The importance of specific input features in the XGBoost models was investigated using variable importance plots (Fig. 4).

Further, the field plots were classified according to their location, presence (and nature) of quaternary deposits, and topography to evaluate if some parts of Sweden's forest landscape were better predicted than others (Fig. 5). Their locations were defined as below or above the highest relict marine coastline (HC) and northern or southern Sweden. Sites and types of quaternary deposits were obtained from the 1:1 000 000 map of quaternary deposits published by the Swedish Geological Survey. Fine sediment is defined as clay and silt while coarse sediment is defined as sand and gravel. Peat refers to areas with at least 30 cm thick peat and bedrock is defined as exposed bedrock with <30 cm thick soil. Standard deviations from the DEM with moving windows of 10 × 10 m and 160 × 160 m were used to define local topography. Values above and below the mean standard deviation of elevation were respectively classified as Steep and Flat (followed by 160 or 10 to indicate the size of moving windows used). Only the 2-class model was evaluated in this manner as the 3- and 5-class models had too few plots in some subcategories. For example, only 11 field plots in the 3-class model were classified as moist-wet on fine sediment.

2.8. Transition from classified to continuous maps

We also tested the possibility of using a probability raster for predicting soil moisture rather than classified data. This can only show the probability for one class at a time. In this study we generated a map showing the probability of each pixel being classified as 'wet'. Clearly, when applying this approach to the 2-class model it can be inferred that cells with a low probability of classification as wet have a higher probability of being dry. Fig. 6 shows the relation between probability values in the resulting map and actual field-classified soil moisture of the

NFI sites. We tested the significance of differences between wetness classes using Kruskal-Wallis tests (Kruskal and Wallis, 1952) and applied Dunn-Bonferroni tests (Dunn, 1961) for *post hoc* comparison of all classes.

2.9. Further evaluation of the ML models in the Krycklan catchment

As well as evaluating ML models' performance statistically, it is highly important to examine maps generated using them visually for inaccuracies related to overfitting and other unrealistic outcomes (Maxwell et al., 2018). Moreover, to evaluate maps rigorously ground truth is clearly essential. Therefore, to complement the statistical assessment described above we visually examined soil moisture maps for the Krycklan catchment – a 68 km^2 experimental site (Lat. 64.150 N, Long. 19.460 E) in northern Sweden (Laudon et al., 2013). The catchment was selected because a large empirical database and numerous previous studies are available for comparison (Kuglerová et al., 2014b; Leach et al., 2017; Ploum et al., 2018; Ågren et al., 2014a, 2015).

In addition to the expert knowledge on the watershed, we exploited data from a forest survey conducted in 2014 including wetness classifications following NFI protocols. The origial survey grid consisted of 500 survey plots with a 10 m radius (314.1 m^2) spaced 350 m apart in the catchment. The plots were positioned using a randomly chosen origin and oriented along coordinate axes of the SWEREF 99 TM projection. Centers of the plots were placed in the field at locations registered within 10 cm using a Trimble GeoXTR GPS receiver. Plots that could not be accurately positioned (where no differential signal could be detected), or plots located on arable land, roads, lakes and plots on or just outside the catchment boundaries were excluded in this study. In total, the Krycklan catchment evaluation dataset consisted of 398 plots with soil moisture classifications. The two evaluation datasets (20% of the NFI plots and 398 plots in the Krycklan Catchment) allowed evaluation of the general predictions for the country and much more detailed tests for a smaller area, with sampling densities of 0.07 and 7.4 plots km^{-1}, respectively. The soil moisture classes in the two field datasets were determined following the same NFI protocol and thus are directly comparable. However, the Krycklan test set has a finer sampling density and provides detailed representation of a specific landscape with gentle topography (elevations ranging from 127 to 372 m a.s.l.) and poorly weathered gnesic bedrock. There are quaternary deposits dominated by glacial till soils in upper parts of the catchment and sorted sediments of sand and silt in lower parts. In terms of land cover, the catchment is dominated by forest (87%) with a mosaic of mires (9%), agricultural land (3%) and lakes (1%) (Laudon et al., 2013).

3. Results

3.1. Performance of the ML algorithms for mapping soil moisture

The performance of the ML algorithms was similar in terms of Kappa and MCC statistics obtained from comparison of predicted and registered soil moisture classes for the NFI plots in the test set. However, we observed some differences in prediction time. XGBoost was the best algorithm, in terms of all measures, while Naïve Bayes models had the lowest Kappa and MCC values, and the Support Vector Machine algorithm was the slowest (it provided models with only 1% lower Kappa and MCC values than XGBoost, but took five times longer to generate them). The Random Forest algorithm took about twice as long to generate predictions, and yielded models with Kappa and MCC values that were 3% lower than those of XGBoost models. However, the Artificial Neural Network approach provided similar performance to the XGBoost algorithm in terms of all three metrics.

3.2. Assessment of the XGBoost classified models

3.2.1. Evaluation of the 5-, 3-, 2-class soil moisture maps using the NFI test plots

Since XGBoost was both the fastest and most accurate of the ML algorithms tested in this study (Table 3), we used it to generate predicted 5-, 3-, and 2-class soil moisture maps then evaluated their accuracy using the test dataset (pertaining to 20% of the NFI field plots). The overall accuracy of the 5-, 3- and 2-class maps was 72, 78, and 85%, respectively, indicating that the 2-class model was the most accurate. This was corroborated by the Kappa values (0.51, 0.58, and 0.69, respectively) and MCC values (0.52, 0.58, and 0.68, respectively). While overall accuracy, Kappa, and MCC statistics provide strong indications of overall model performance, it is also important to evaluate the accuracy of specific classes for multi-class predictions. Thus, recall and F1 values were calculated for the classes in each of the classified maps (Table 4). Recall values were low for wet (32%) and dry (19%) classes in the 5-class model, but higher (suggesting reasonable accuracy) for the mesic, mesic-moist, and moist classes. Similarly, F1 values of the 5-class model suggested that its wet and dry class predictions may not be sufficiently accurate for operational purposes. In contrast, recall and F1 values for all the classes in the 3-class and 2-class models indicated sufficient accuracy (≥58% and 0.59, respectively). The values were substantially lower for the mesic-moist, and moist-wet classes of the 3-class model than for the dry-mesic class in that model and both classes of the 2-class model. However, the 3-class model could still have some advantages over the 2-class model for effective planning in practical forestry and land management. In addition to the model performance measures presented here, many others (including confusion matrixes) were calculated and are reported in SI 1–3.

3.2.2. Assessment of feature importance

We evaluated the importance of all the input features utilized in the XGBoost generation of 5-, 3-, and 2-class models. The DTW index with different flow accumulation thresholds, TWI from a 10 m DEM, and currently mapped wetlands were the most important predictors for all models (Fig. 4). Overall, the LIDAR-derived terrain indices were the most important predictors, as expected. Summer and autumn runoff, peat soil layer, and Y coordinate were also strong predictors. The latitudinal variation from north to south, as reflected by the Y coordinate, strongly influenced the soil moisture distribution across Sweden. Interestingly, surficial geological information (e.g. distributions of till, fine sediment, and thin soil) were less important for the predictions. The small-scale topographical measures did not have high VIP scores, but contributed somewhat to the model (STDV 5 cells most strongly).

3.2.3. Location-specific accuracy assessment of the generated maps

As well as evaluating the accuracy of the maps generated by the models against registered data for the test set of 20% NFI plots (see section 3.2.1), we investigated if predictions were better for some parts of Sweden's forest landscape than others. For this, we used MCC values of the 2-class model (Fig. 5). We detected marginal effects of the plots' location as the model performed slightly better for plots in the north and below the highest relict coastline than for those in the south and higher than the coastline, respectively (Fig. 5A). Quaternary deposits had mixed effects, as the model performed better for plots with glacial till and peat soils than for plots on coarse sediments (Fig. 5B). However, the local slope (at various scales) had the strongest effect on model performance, with better accuracy for flat terrain than steep terrain (Fig. 5C). For example, the MCC value was 0.26 higher for plots in Flat 160 terrain than for plots in Steep 10 terrain (as defined in section 2.7).

3.3. Transition from classified to continuous maps

Analysis of the continuous map of soil moisture at the NFI sites generated, from the 2-class model using the probability raster are

Table 4

Performance of the 5-, 3-, 2-class models for predicting soil moisture in the test set of NFI field plots. Kappa and MCC refer to Cohen's Kappa Coefficient and Matthews Correlation Coefficient, respectively. Recall (sensitivity) and F1 (the harmonic mean of sensitivity and precision) are measures of sensitivity and precision of specific predicted classes.

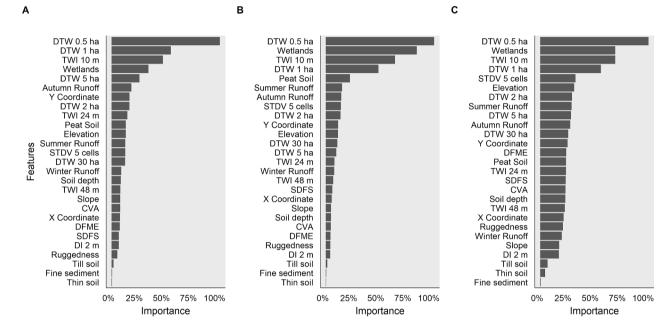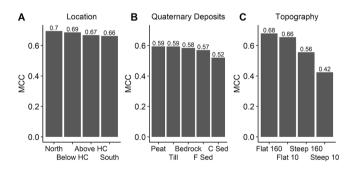| 5-class model (Kappa 0.51, MCC 0.52)			3-class model (Kappa 0.58, MCC 0.58)			2-class model (Kappa 0.69, MCC 0.68)		
Classes	Recall	F1	Classes	Recall	F1	Classes	Recall	F1
Dry	19%	0.28	Dry-Mesic	90%	0.88	'Dry'	89%	0.88
Mesic	89%	0.84						
Mesic-moist	60%	0.61	Mesic - moist	58%	0.59	'Wet'	79%	0.81
Moist	46%	0.51	Moist-wet	59%	0.64			
Wet	32%	0.41						

Fig. 4. Variable importance of the 28 input features for the 2-class (A), 3-class (B), and (C) 5- class XGBoost models. The variable names are explained in Table 2. Note that the variable Coarse sediment was removed from the graph, as it was so close to 0 that the column became invisible.

Fig. 5. Performance values (Matthews Correlation Coefficients) of the 2-class model for plots at different locations (A), on various quaternary deposits (B), and with different topography (C). HC, C sed, F Sed, refer to high coastline, coarse sediment, and fine sediment, respectively. Flat 160, Steep 10, Steep 160 and Steep 10 refer to flat and steep terrain determined with 160 m × 160 m and 10 m × 10 m moving windows. See section 2.7 for definitions.

presented in Fig. 6, which shows that Wet and Dry plots (blue and red boxes, respectively) had high and low probabilities of being classified as wet by the model. Probability ranges were narrow for Dry and Wet plots, while probabilities for the Mesic-Moist plots ranged from 0 to 100% but most fell in the middle range between mesic and moist. While there was some overlap between the classes generally, the probability map seems to capture the variation in soil moisture rather well. The Kruskal-Wallis test followed by the Dunn-Bonferroni test showed significant differences
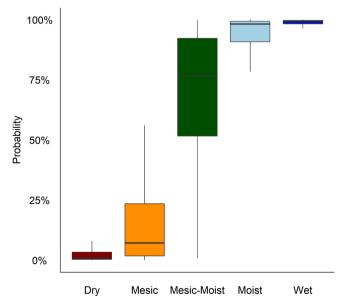

Fig. 6. Boxplot of probabilities of National Forest Inventory (NFI) test plots being classified as wet by the two-class model. The Kruskal-Wallis test followed by the Dunn-Bonferroni test showed that all five classes significantly differed (p < 0.05).

between all classes.

3.4. Further evaluation of the 5-, 3-, and 2-class models in the Krycklan catchment

Further evaluation of the 5-, 3-, 2-class models using 398 test plots in the Krycklan catchment resulted in similar performance patterns to the national patterns (Table 4). However, their predictions for the catchment were generally poorer. Recall and F1 values of the dry and wet classes highlight the uncertainty of the 5-class model (Table 5, Fig. 7C). However, the 3-class model performed reasonably well in the Krycklan catchment (Fig. 7B). In fact, the dry-mesic and moist-wet classes were predicted with equally high or higher recall and F1 values to those obtained in the national evaluation, but the mesic-moist class had relatively low recall and F1 measures (Tables 4 & 5). Recall and F1 values for the 2-class model's predictions for the catchment and NFI test plots were similar. However, there was a stark contrast in estimates of overall model accuracy between the two evaluations, especially for the 5-class model (for which the Kappa and MCC values were 0.28 and 0.29 lower, respectively, for the Krycklan catchment than for the national-level predictions reported in Table 4). Similarly, Kappa and MCC values of the 3-class and 2-class models' predictions were relatively low for the Krycklan catchment. These findings corroborated the finding that soil moisture class was predicted more accurately in some parts of Sweden's forest landscape than others (Fig. 5).

Fig. 7 shows the maps generated from the 2-, 3- and 5-class models and the probability map for Krycklan catchment. The maps show quite good agreement with the field measurements (which is more clearly displayed with higher zooming than possible here). For details of the maps' accuracy see Table 5. The maps show quite good agreement with the field measurements (which is more clearly displayed with higher zooming than possible here).

4. Discussion

For decades, researchers have been developing terrain indices for modelling soil moisture (Beven and Kirkby, 1979; Hjerdt et al., 2004; Meles et al., 2020; Murphy et al., 2008; Rennó et al., 2008). Identifying optimal thresholds and spatial scales for predicting soil moisture in different regions has remained a major constraint and cause of prediction uncertainty (Sørensen and Seibert, 2007; Ågren et al., 2014b). However, recent studies have demonstrated the potential of using ML techniques in combination with large sets of digital terrain indices for mapping soil drainage (Goldman et al., 2020), wetlands (Maxwell et al., 2016) and wet areas (Lidberg et al., 2020) over large regions at high spatial resolution. In the study reported here we extended the work of Lidberg et al. (2020) by utilizing additional predictor variables using several LIDAR-derived topographical indices (with various scales and thresholds) and a set of ML algorithms, including one that has not been widely used for soil mapping, XGBoost (Chen and Guestrin, 2016), and also investigate multi-class and continuous soil moisture models. We obtained models that provided high-resolution (2 × 2 m) soil moisture maps and more accurate predictions than those obtained by Lidberg et al. (2020), e.g., a 2-class model covering the entire Swedish forest landscape with a Kappa value of 0.69 and overall accuracy of 85%. Thus, our approach can enhance the utility of ML algorithms for high-resolution soil moisture modelling using LIDAR-derived terrain indices. We also corroborated the utility of the relatively new XGBoost algorithm for environmental modelling, in accordance with previous studies on similar topics (Georganos et al., 2018; Jia et al., 2019; Nielsen, 2016). Before working with ML models we tried to develop regression models (based, for example, on logistic regression and several multivariate methods) to adjust the maps to local conditions, but we were not successful. Thus, although ML requires numerous samples and intensive computation we found that it provided much more accurate models than regression models. Several other authors (Chen et al., 2019;

Nussbaum et al., 2018) have also reported that ML models provide better predictions than geostatistical and statistical approaches, especially for regional-scale analyses of heterogeneous landscapes.

With ongoing increases in climatic variability and consequent complexity of land management, landscape-scale soil moisture maps have become extremely important for effective management of natural resources. While maps based on satellite data can capture the temporal variability of soil moisture (through up to ca. 3.5 scans per week), poor spatial resolution often limits their utility for practical applications (Zeng et al., 2019). Moreover, tree canopies in forested landscapes can severely hinder soil moisture measurements by satellite remote sensing (Gao et al., 2017), and thus reduce the accuracy of satellite-based soil moisture maps. We incorporated land use information derived from SENTINEL-2 satellite images with 10 m spatial resolution acquired in the European earth observation program Copernicus (Table 2), but they were subsequently excluded due to low importance. Therefore, we concluded that LIDAR-derived terrain indices are stronger predictors of landscape-scale variation in soil moisture, and ML modeling based on the indices can provide accurate, spatially extensive, high-resolution soil moisture maps.

In a recent Canadian study the ML algorithm Random Forest was used to predict a 5-class natural soil drainage map from high-resolution LIDAR-derived digital terrain indices (Goldman et al., 2020). The model obtained, for a Canadian wetland forest landscape, had lower overall accuracy (70%) and Kappa value (0.54) than the best models we obtained. While a similar overall approach was applied in both studies, several methodological differences may have contributed to the differences in prediction accuracy. For example, Goldman et al. (2020) extracted indices from a 3 m resampled DEM instead of a 2 m DEM as we did, and only used the Random Forest algorithm, while we found that XGBoost provided the best models of four evaluated ML algorithms (including Random Forest). Another major difference between the studies was in the training datasets, as we utilized data pertaining to 19,643 field plots at locations recorded with 5–10 m accuracy by a Differential Global Positioning System (DGPS) system, while Goldman et al. (2020) applied field data from 382 pedon descriptions, with estimated locations based on handwritten notes and/or points indicated in aerial photographs. Moreover, DTW was the most important feature in our study but it was not evaluated in the Canadian study. Thus, we concluded that to obtain accurate predictions of soil moisture over extensive landscapes it is important to: test a group of ML algorithms rather than relying on one; use the most informative, high-resolution terrain indices as input features; and apply large datasets with highly accurately located and extensively distributed field plots. However, there is a misconception among non-experts that expensive field measurement programs can be completely replaced with remote sensing observations and ML models for environmental monitoring. In reality, ML approaches are excellent for upscaling and generating wall-to-wall maps based on point observations, but the success of any ML model hinges on the quality and size of the field datasets (Biswas and Zhang, 2018). Thus, we urge decision-makers to expand field measurement programs to strengthen the ML-based prediction of environmental parameters, including soil moisture.
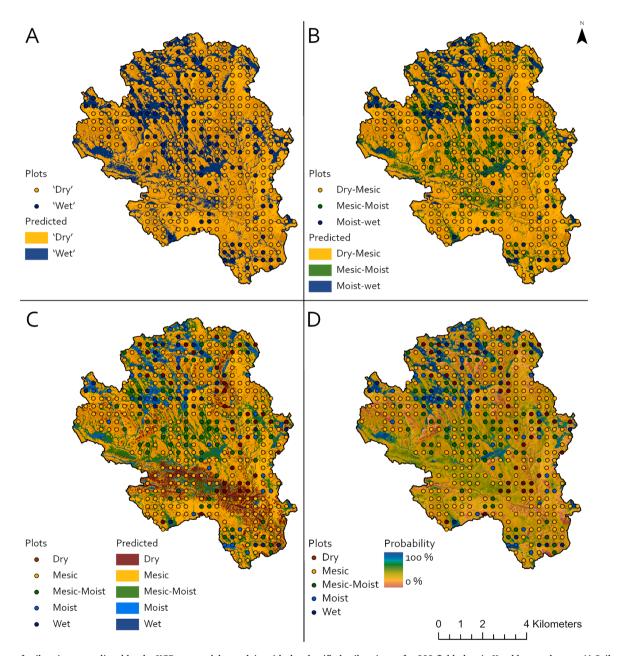
4.1. Evaluation of classified models

To increase the applicability of the digital classified soil moisture maps in practical land-use management, it is important to predict soil moisture across the whole range from dry to wet. Hence, we produced several multi-class (5-, 3-, and 2-class) soil moisture maps capturing the whole spectrum of soil wetness in the Swedish forest landscape. When constructing classification models the relative costs of omitting and over-predicting classes depend on the context and applications. For example, in cancer research it is better to accept some over-prediction (false positives) to avoid missing any cancerous cells (true positives). However, as we are equally interested in all soil moisture classes, we

Table 5

Performance of the ML models when applied to the field plots in Krycklan catchment. All models provided less accurate soil predictions for the catchment than the national-scale predictions.

5-class model (Kappa 0.23, MCC 0.23)			3-class model (Kappa 0.46, MCC 0.47)			2-class model (Kappa 0.56, MCC 0.57)		
Class	Recall	F1	Class	Recall	F1	Class	Recall	F1
Dry	13%	0.15	Dry-Mesic	83%	0.88	'Dry'	81%	0.67
Mesic	72%	0.75						
Mesic-moist	48%	0.43	Mesic - moist	46%	0.56	'Wet'	83%	0.88
Moist	20%	0.16	Moist-wet	82%	0.49			
Wet	0%	–						

Fig. 7. Maps of soil moisture predicted by the XGBoost models overlain with the classified soil moisture for 398 field plots in Krycklan catchment. A) Soil moisture predicted in two classes ('Dry' and 'Wet'), B) Soil moisture predicted in three classes, C) Soil moisture predicted in five classes. D) Probability of wet classification (0–100%) from the 2-class model. The classified models are defined in Table 1.

value recall and precision equally, so Kappa values are suitable measures of performance as they provide balanced indications in this respect. The findings that the 2-class map was the most accurate and 5-class map the least accurate, in terms of Kappa, were consistent with expectations as the risk of mis-classifying a pixel increases with the number of classes. In

addition, we obtained very low Recall and F1 values for dry and wet classes in the 5-class model (Tables 3 and 4), probably because few field plots of these classes were available for the modeling (Fig. 3). A common approach for dealing with such issues is to generate a balanced dataset by under-sampling from the dominant classes (Chicco, 2017), but in our

case that would have left too few samples to represent the Swedish forest landscape. Instead, we argue that a better approach is to merge poorly-represented classes, as the recall and F1 values may be much better for the combined classes (as we found when we generated a 3-class model from our 5-class model). Kappa values have been considered better measures for imbalanced datasets (Fig. 3) than overall accuracy and they are widely used in evaluations of maps. Recently, however, it has been shown that Kappa also exhibits an undesired behavior on unbalanced datasets (Delgado and Tibau, 2019). The MCC is the most reliable statistical measure as it is only high if the predictions are good in terms of all four confusion matrix categories (true positives, false negatives, true negatives, and false positives). Therefore, MCC provides the most informative and truthful measure for evaluating binary (Chicco and Jurman, 2020), and multi-class classifications (Delgado and Tibau, 2019). Hence, in our detailed analysis of the predictions for different parts of Sweden's forest landscape we focused solely on MCC values (Fig. 5). However, it should be noted that for most cases Kappa and MCC values were identical (Table 3), indicating that lack of balance in the dataset did not seriously influence Kappa values in our study.

In addition, the 2-class model was further analyzed to investigate potential variations in its performance associated with variations in sites' locations, quaternary deposits, and topographic settings (Fig. 5). We found that there was no large bias along the latitudinal gradient, or above/below the highest relict coastline (Fig. 5A), indicating that the 2-class model adapted the map to climatic gradients from north to south and along the elevation gradient from the Caledonian mountains in the northwest to the low-lying areas in the south and east. However, the model's performance was influenced by the quaternary deposits (Fig. 5B), in accordance with expectations as many of the input digital terrain indices (e.g. DTW, TWI, DI) are based on the assumption that topography controls groundwater flowpaths (Rinderer et al., 2014). Such an assumption is usually valid for soils with low hydraulic conductivity, for example, glacial till soils and fine sediments where most of the groundwater flowpaths are in upper levels of the soils (Beven and Germann, 2013; Nyberg et al., 1999). However, coarse sediments have much higher hydraulic conductivity, enabling deeper infiltration of water, which decreases the topographical control on groundwater flows and thus could explain the poorer model performance (MCC, 0.52) for plots on coarse sediments (Fig. 5B). The model performance was poorest in areas where the local topography was steep (MCC, 0.42), which provides potentially important indications for practitioners that the developed maps should be used with caution for sites on coarse sediments and steep terrain.

The finding that modeling of soil moisture in the Krycklan catchment (Table 5) was poorer than the national mapping (Table 4) was probably due to the large amounts of coarse sediments in the lower part of the catchment (Fig. 7), as predictions for sites on such sediments were relatively poor across the country (cf. Fig. 5B). Remnants of a large post-glacial delta cover most of the low-lying part of the catchment, mostly consisting of sand and silt, which hinders accurate soil moisture modeling. Models often predict that this area is wetter than the empirical records suggest, because an assumption underlying many digital terrain indexes is that flat areas are wetlands (Grabs et al., 2009). However, the 5-class model seemed to overcompensate for the sediment effects, and predicted that some areas were drier, and others wetter, than in reality (Fig. 7C). The relatively poor predictions for this unusually large flat area with contrastingly coarse soils is likely the main reason for the difference in model performance with the national dataset (Table 4) and Krycklan dataset (Table 5).
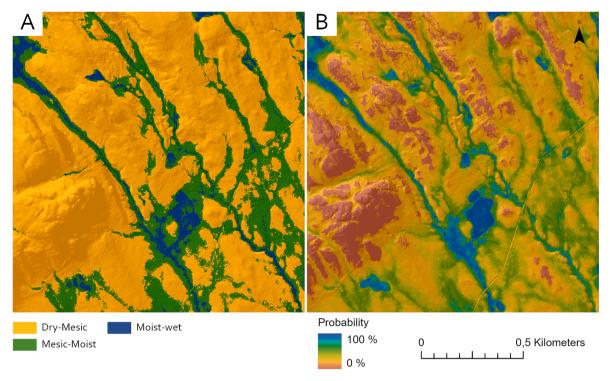
Another shortcoming of the maps was observed while viewing the map of the Krycklan catchment on-screen, which revealed inconsistencies at the road-stream intersections. This is a known issue when working with high-resolution DEMs, in which roads are elevated above the surrounding terrain causing roadside impoundments in the models. This issue could be partially resolved during the preprocessing and calculation of the digital terrain indices. We previously found that

breaching the Swedish national DEM produced the best outcomes for hydrological calculations (Lidberg et al., 2017). Despite utilizing this approach in the study presented here, we found inconsistencies at approximately 25% of the road-stream intersections in the Krycklan catchment, based on our expert knowledge from a field survey of all culverts in the catchment.

DTW maps have contributed to significant changes in various aspects of forest management, such as: placement of access roads and extraction road networks, wood landing sites, and stream crossings; division into summer and winter harvest blocks; judging if logging residues are needed for ground protection or can be harvested for bioenergy; protection of riparian zones during fertilization; and site preparation (Mohtashami et al., 2017; Murphy et al., 2008; Ring et al., 2020; White et al., 2012; Ågren et al., 2015). However, although they have major advantages over conventional maps for efficient land-use management, they have some important limitations (Lidberg et al., 2020; Ågren et al., 2014b). *Inter alia*, calculation of DTW maps involves selection of a specific threshold for stream initiation, while in reality the threshold varies substantially both locally and regionally (Elmore et al., 2013; Jaeger et al., 2019; Jensen et al., 2017; Julian et al., 2012; Ågren et al., 2014). Here we calculated the digital terrain indices using diverse thresholds and the XGBoost model to adapt the maps to different landscapes, thereby combining use of the NFI field dataset and ML to enable data-driven improvement of the soil moisture mapping. Comparison of the 2-class XGBoost map with a 2-class DTW map (Lidberg et al., 2020), using data pertaining to 20% of the NFI plots, shows that this approach improved overall accuracy from 79% to 85% and the Kappa value from 0.56 to 0.69.

4.2. Transition from classified to continuous maps

Categorization is a fundamental mechanism of human construction of knowledge of the world (McGarty, 2015). By learning which category a soil belongs to, one also learns about relationships between soils. However, in nature there are no clear boundaries between soil moisture classes (as indicated by the map in Fig. 8A). The categories refer to average soil moisture conditions for sets of sites, while in reality soil moisture varies seasonally depending on local weather conditions, and both stream networks and associated areas of wet soils expand and shrink during the year (Jaeger et al., 2019; Lyon et al., 2004; Quinn and Beven, 1993; Ågren et al., 2015). The ML method XGBoost can also generate maps of the probability of each pixel being classified as wet. Similar probability maps have been used to classify soil moisture in Alberta, Canada (Delancey et al., 2019; Hird et al., 2017). However, instead of classifying it, using a multicolored map with smooth transitions between the colors makes it easier for practitioners to infer this seasonal variability. In simplified terms, NFI defines wet and moist areas as those that have a shallow water table and are wet most of the year (with peat accumulation and species that thrive in wet conditions), while moist-mesic soils are seasonally wet following snowmelt or rain. In practice, this means that blue and turquoise areas in Fig. 7B are more or less wet throughout the year while green areas have high groundwater levels and high hydrological connectivity during high-flow periods. Therefore, it is more rational to utilize raw probability maps for practical management (Fig. 8B), such as wetland restoration (Goldman et al., 2020) or forestry operations (Murphy et al., 2008). In efforts to facilitate application of our results in practice and provide better planning tools for land-use management in Sweden both maps in Fig. 8 were released as open geodata for all of Sweden (www.slu.se/mfk). Future further development of this national scale soil moisture map could entail incorporation of distance to ditches data (O'Neil et al., 2020), but most of the ditch networks in Sweden have not been mapped (Kuglerová et al., 2017).

Finally, it should be noted that calculation of soil moisture on a 2 m DEM requires substantial data storage and processing power. For some landscapes it may be worth aggregating the DEMs to the order of 5, 10 or

Fig. 8. Illustrative map of the Krycklan catchment, with slightly transparent soil moisture maps superimposed on the hillshade of the 2 m digital elevation model. A) Soil moisture predicted in three classes using Extreme Gradient Boosting (XGBoost). B) Probability of wet classification (0–100%) based on the 2-class model obtained using XGBoost.

even 15 m resolution, to reduce the amount of data and these requirements. However, according to a recent study, the average width (±SE) of retained forest buffers along streams was 15.9 ± 2.1 m in British Columbia, 15.3 ± 1.4 m in Finland, and just 4 ± 0.4 m in Sweden (Kuglerová et al., 2020). Thus, as one of the main purposes of the developed maps is to provide planning tools for hydrologically adapted protection zones (Kuglerová et al., 2014) we had to maintain very high resolution (2 m) to derive a relevant soil moisture map for practical forest management in Sweden.

5. Conclusions

LIDAR-derived terrain indices and ML models provided an effective and accurate approach for modeling soil moisture in the Swedish forest landscape at high spatial resolution (2 × 2 m). We tested multiple ML methods, including Artificial Neural Network, Random Forest, Support Vector Machine, Naïve Bayes classification, and Extreme Gradient Boosting (XGBoost, which provided the best predictions in terms of both accuracy and prediction time). We generated a 3-class soil moisture map with sufficient quality for use in practical land use management. We also generated a 5-class map, which did not have enough training data in the wet and dry classes to provide reasonably accurate predictions. However, for practical forest management we argue that the probability map, showing predictions of soil moisture from 0% (dry) to 100% (wet), provided more valuable information. The 3-class map and probability map we produced have been released for practitioners. While the probability map outperforms other available soil moisture maps, it should be used with caution near roads, at sites on coarse sediments, and in areas with steep local topography.

Declaration of Competing Interest

The authors declare that they have no known competing financial interests or personal relationships that could have appeared to influence the work reported in this paper.

References

Ågren, A.M., Buffam, I., Cooper, D.M., Tiwari, T., Evans, C.D., Laudon, H., 2014a. Can the heterogeneity in stream dissolved organic carbon be explained by contributing landscape elements? Biogeosciences 11 (4), 1199–1213. https://doi.org/10.5194/bg-11-1199-2014.
Ågren, A.M., Lidberg, W., Ring, E., 2015. Mapping Temporal Dynamics in a Forest Stream Network-Implications for Riparian Forest Management. Forests 6 (9), 2982–3001. https://doi.org/10.3390/f6092982.
Ågren, A.M., Lidberg, W., Strömgren, M., Ogilvie, J., Arp, P.A., 2014b. Evaluating digital terrain indices for soil wetness mapping - a Swedish case study. Hydrol. Earth. Syst. Sc. 18 (9), 3623–3634. https://doi.org/10.5194/hess-18-3623-2014.
Akumu, C.E., Baldwin, K., Dennis, S., 2019. GIS-based modeling of forest soil moisture regime classes: Using Rinker Lake in northwestern Ontario, Canada as a case study. Geoderma 351, 25–35. https://doi.org/10.1016/j.geoderma.2019.05.014.
Ali, I., Greifeneder, F., Stamenkovic, J., Neumann, M., Notarnicola, C., 2015. Review of Machine Learning Approaches for Biomass and Soil Moisture Retrievals from Remote Sensing Data. Remote Sens. 7 (12), 16398–16421. https://doi.org/10.3390/rs71215841.
Bauer-Marschallingere, B., Freeman, V., Cao, S., Paulik, C., Schaufler, S., Stachl, T., Modanesi, S., Massario, C., Ciabatta, L., Brocca, L., Wagner, W., 2019. Toward Global Soil Moisture Monitoring With Sentinel-1: Harnessing Assets and Overcoming Obstacles. IEEE Trans. Geosci. Remote. Sens. 57 (1), 520–539. https://doi.org/10.1109/TGRS.2018.2858004.
Beven, K., Germann, P., 2013. Macropores and water flow in soils revisited. Water Resour. Res. 49 (6), 3071–3092. https://doi.org/10.1002/wrcr.20156.
Beven, K.J., Kirkby, M.J., 1979. A physically based, variable contributing area model of basin hydrology / Un modèle à base physique de zone d'appel variable de l'hydrologie du bassin versant. Hydrol. Sci. B. 24 (1), 43–69. https://doi.org/10.1080/02626667909491834.
Bhargavi, P., Jyothi, S., 2009. Applying Naive Bayes Data Mining Techinque for Classification of Agricultural Land Soils. IJCSNS International Journal of Computer Science and Network Security 9, 117–122.
Biswas, A., Zhang, Y.K., 2018. Sampling Designs for Validating Digital Soil Maps: A Review. Pedosphere 28 (1), 1–15. https://doi.org/10.1016/S1002-0160(18)60001-3.
Breiman, L., 2001. Random forests. Mach. Learn. 45 (1), 5–32. https://doi.org/10.1023/A:1010933404324.

Chang, C.-C., Lin, C.-J., 2011. LIBSVM: A library for support vector machines. ACM Trans. Intell. Syst. Technol. 2 (3), 27. https://doi.org/10.1145/1961189.1961199.

Chen, L., Ren, C.Y., Li, L., Wang, Y.Q., Zhang, B., Wang, Z.M., Li, L.F., 2019. A Comparative Assessment of Geostatistical, Machine Learning, and Hybrid Approaches for Mapping Topsoil Organic Carbon Content. Isprs. Int. J. Geo-Inf. 8 (4), 27. https://doi.org/10.1145/1961189.1961199.

Chen, T., Guestrin, C., 2016. XGBoost: A Scalable Tree Boosting System, Proceedings of the 22nd ACM SIGKDD International Conference on Knowledge Discovery and Data Mining. Association for Computing Machinery, San Francisco, California, USA, pp. 785–794.

T. Chen T. He M. Benesty V. Khotilovich Y. Tang H. Cho K. Chen R. Mitchell I. Cano T. Zhou M. Li J. Xie M. Lin Y. Geng Y. Li Xgboost: Extreme Gradient Boosting 2020 R package version 1.0.0.2.

Chicco, D., 2017. Ten quick tips for machine learning in computational biology. Biodata Min. 10 https://doi.org/10.1186/s13040-017-0155-3.

Chicco, D., Jurman, G., 2020. The advantages of the Matthews correlation coefficient (MCC) over F1 score and accuracy in binary classification evaluation. BMC Genomics 21 (1), 6. https://doi.org/10.1186/s12864-019-6413-7.

Cohen, J., 1960. A Coefficient of Agreement for Nominal Scales. Educ. Psychol. Meas. 20 (1), 37–46. https://doi.org/10.1177/001316446002000104.

Delancey, E.R., Kariyeva, J., Bried, J.T., Hird, J.N., 2019. Large-scale probabilistic identification of boreal peatlands using Google Earth Engine, open-access satellite data, and machine learning. Plos One 14 (6), e0218165. https://doi.org/10.1371/journal.pone.0218165.

Delgado, R., Tibau, X.A., 2019. Why Cohen's Kappa should be avoided as performance measure in classification. Plos One 14 (9), e0222916. https://doi.org/10.1371/journal.pone.0222916.

Dunn, O.J., 1961. Multiple Comparisons among Means. J. Am. Stat. Assoc. 56(293), 52–64. https://doi.org/ 10.1080/01621459.1961.10482090.

Edwards, G., White, D.R., Munkholm, L.J., Sørensen, C.G., Lamande, M., 2016. Modelling the readiness of soil for different methods of tillage. Soil Till. Res. 155, 339–350. https://doi.org/10.1016/j.still.2015.08.013.

El Hajj, M., Baghdadi, N., Zribi, M., Bazzi, H., 2017. Synergic Use of Sentinel-1 and Sentinel-2 Images for Operational Soil Moisture Mapping at High Spatial Resolution over Agricultural Areas. Remote Sens. 9 (12), 1292. https://doi.org/10.3390/rs9121292.

Erdozain, M., Emilson, C.E., Kreutzweiser, D.P., Kidd, K.A., Mykytczuk, N., Sibley, P.K., 2020. Forest management influences the effects of streamside wet areas on stream ecosystems. Ecol. Appl. 30 (4), e02077 https://doi.org/10.1002/eap.2077.

Fridman, J., Holm, S., Nilsson, M., Nilsson, P., Ringvall, A.H., Stahl, G., 2014. Adapting National Forest Inventories to changing requirements - The case of the Swedish National Forest Inventory at the turn of the 20th century. Silva Fenn. 48 (3), 1–29. https://doi.org/10.14214/sf.1095.

Gao, Q., Zribi, M., Escorihuela, M.J., Baghdadi, N., 2017. Synergetic Use of Sentinel-1 and Sentinel-2 Data for Soil Moisture Mapping at 100 m Resolution. Sensors-Basel 17 (9), 1966. https://doi.org/10.3390/s17091966.

Georganos, S., Grippa, T., Vanhuysse, S., Lennert, M., Shimoni, M., Wolff, E., 2018. Very High Resolution Object-Based Land Use-Land Cover Urban Classification Using Extreme Gradient Boosting. IEEE Geosci. Remote S. 15 (4), 607–611. https://doi.org/10.1109/LGRS.2018.2803259.

Goldman, M.A., Needelman, B.A., Rabenhorst, M.C., Lang, M.W., McCarty, G.W., King, P., 2020. Digital soil mapping in a low-relief landscape to support wetland restoration decisions. Geoderma 373, 114420. https://doi.org/10.1016/j.geoderma.2020.114420.

Grabs, T., Seibert, J., Bishop, K., Laudon, H., 2009. Modeling spatial patterns of saturated areas: A comparison of the topographic wetness index and a dynamic distributed model. J. Hydrol. 373 (1–2), 15–23. https://doi.org/10.1016/j.jhydrol.2009.03.031.

Hird, J.N., DeLancey, E.R., McDermid, G.J., Kariyeva, J., 2017. Google Earth Engine, Open-Access Satellite Data, and Machine Learning in Support of Large-Area Probabilistic Wetland Mapping. Remote Sens. 9 (12), 1315. https://doi.org/10.3390/rs9121315.

Hjerdt, K.N., McDonnell, J.J., Seibert, J., Rodhe, A., 2004. A new topographic index to quantify downslope controls on local drainage. Water Resour. Res. 40 (5), W05602. https://doi.org/10.1029/2004WR003130.

Jaeger, K.L., Sando, R., McShane, R.R., Dunham, J.B., Hockman-Wert, D.P., Kaiser, K.E., Hafen, K., Risley, J.C., Blasch, K.W., 2019. Probability of Streamflow Permanence Model (PROSPER): A spatially continuous model of annual streamflow permanence throughout the Pacific Northwest. J. Hydrol. X 2, 100005. https://doi.org/10.1016/j.hydroa.2018.100005.

Jensen, C.K., McGuire, K.J., Prince, P.S., 2017. Headwater stream length dynamics across four physiographic provinces of the Appalachian Highlands. Hydrol. Process. 31 (19), 3350–3363. https://doi.org/10.1002/hyp.11259.

Jia, Y., Jin, S.G., Savi, P., Gao, Y., Tang, J., Chen, Y.X., Li, W.M., 2019. GNSS-R Soil Moisture Retrieval Based on a XGboost Machine Learning Aided Method: Performance and Validation. Remote Sens. 11 (14), 1655. https://doi.org/10.3390/rs11141655.

Kruskal, W.H., Wallis, W.A., 1952. Use of Ranks in One-Criterion Variance Analysis. Journal of the American Statistical Association 47 (260), 583–621. https://doi.org/10.2307/2280779.

Kuglerová, L., Ågren, A., Jansson, R., Laudon, H., 2014a. Towards optimizing riparian buffer zones: Ecological and biogeochemical implications for forest management. Forest Ecol. Manag. 334, 74–84. https://doi.org/10.1016/j.foreco.2014.08.033.

Kuglerová, L., Hasselquist, E.M., Richardson, J.S., Sponseller, R.A., Kreutzweiser, D.P., Laudon, H., 2017. Management perspectives on Aqua incognita: Connectivity and cumulative effects of small natural and artificial streams in boreal forests. Hydrol. Process. 31 (23), 4238–4244. https://doi.org/10.1002/hyp.11281.

Kuglerová, L., Jansson, R., Ågren, A., Laudon, H., Malm-Renöfält, B., 2014b. Groundwater discharge creates hotspots of riparian plant species richness in a boreal forest stream network. Ecology 95 (3), 715–725. https://doi.org/10.1890/13-0363.1.

M. Kuhn J. Wing S. Weston A. Williams C. Keefer A. Engelhardt Caret: Classification and regression training 2012 https://Cran.R-Project.Org/Package=Caret.

Laudon, H., Taberman, I., Ågren, A., Futter, M., Ottosson-Löfvenius, M., Bishop, K., 2013. The Krycklan Catchment Study-A flagship infrastructure for hydrology, biogeochemistry, and climate research in the boreal landscape. Water Resour. Res. 49 (10), 7154–7158. https://doi.org/10.1002/wrcr.20520.

Leach, J.A., Lidberg, W., Kuglerová, L., Peralta-Tapia, A., Ågren, A., Laudon, H., 2017. Evaluating topography-based predictions of shallow lateral groundwater discharge zones for a boreal lake-stream system. Water Resour Res 53 (7), 5420–5437. https://doi.org/10.1002/2016WR019804.

Leempoel, K., Parisod, C., Geiser, C., Dapra, L., Vittoz, P., Joost, S., 2015. Very high-resolution digital elevationmodels: Are multi-scale derived variables ecologically relevant? Methods Ecol. Evol. 6 (12), 1373–1383. https://doi.org/10.1111/2041-210X.12427.

Lidberg, W., Nilsson, M., Ågren, A., 2020. Using machine learning to generate high-resolution wet area maps for planning forest management: A study in a boreal forest landscape. Ambio 49 (2), 475–486. https://doi.org/10.1007/s13280-019-01196-9.

Lidberg, W., Nilsson, M., Lundmark, T., Ågren, A.M., 2017. Evaluating preprocessing methods for hydrological modelling of digital elevation models. Hydrol. Process. 31 (26), 4660–4668. https://doi.org/10.1002/hyp.11385.

Lindsay, J.B., 2016. Efficient hybrid breaching-filling sink removal methods for flow path enforcement in digital elevation models. Hydrol. Process. 30 (6), 846–857. https://doi.org/10.1002/hyp.10648.

Lindsay, J.B., 2020. WhiteboxTools User Manual. University of Guelph Guelph, Canada, Geomorphometry and Hydrogeomatics Research Group.

Lyon, S.W., Walter, M.T., Gerard-Marchant, P., Steenhuis, T.S., 2004. Using a topographic index to distribute variable source area runoff predicted with the SCS curve-number equation. Hydrol. Process. 18 (15), 2757–2771. https://doi.org/10.1002/hyp.1494.

Matthews, B.W., 1975. Comparison of the predicted and observed secondary structure of T4 phage lysozyme. Biochimica et Biophysica Acta (BBA) - Protein. Structure 405 (2), 442–451. https://doi.org/10.1016/0005-2795(75)90109-9.

Maxwell, A.E., Warner, T.A., Fang, F., 2018. Implementation of machine-learning classification in remote sensing: An applied review. Int. J. Remote Sens. 39 (9), 2784–2817. https://doi.org/10.1080/01431161.2018.1433343.

Maxwell, A.E., Warner, T.A., Strager, M.P., 2016. Predicting Palustrine Wetland Probability Using Random Forest Machine Learning and Digital Elevation Data-Derived Terrain Variables. Photogramm. Eng. Rem. S. 82 (6), 437–447. https://doi.org/10.1016/S0099-1112(16)82038-8.

McGarty, C., 2015. Social Categorization. International Encyclopedia of the Social & Behavioral Sciences 186–191. https://doi.org/10.1093/acrefore/9780190236557.013.308.

Meles, M.B., Younger, S.E., Jackson, C.R., Du, E.H., Drover, D., 2020. Wetness index based on landscape position and topography (WILT): Modifying TWI to reflect landscape position. J. Environ. Manage. 255 (4), 109863 https://doi.org/10.1016/j.jenvman.2019.109863.

Mohanty, B.P., Cosh, M.H., Lakshmi, V., Montzka, C., 2017. Soil Moisture Remote Sensing: State-of-the-Science. Vadose Zone J. 16 (1), 1–9. https://doi.org/10.2136/vzj2016.10.0105.

Mohtashami, S., Eliasson, L., Jansson, G., Sonesson, J., 2017. Influence of soil type, cartographic depth-to-water, road reinforcement and traffic intensity on rut formation in logging operations: A survey study in Sweden. Silva Fenn. 51 (5), 2018. https://doi.org/10.14214/sf.2018.

Murphy, P.N.C., Ogilvie, J., Castonguay, M., Zhang, C.F., Meng, F.R., Arp, P.A., 2008. Improving forest operations planning through high-resolution flow-channel and wet-areas mapping. Forest Chron 84 (4), 568–574. https://doi.org/10.5558/tfc84568-4.

Murphy, P.N.C., Ogilvie, J., Connor, K., Arpl, P.A., 2007. Mapping wetlands: A comparison of two different approaches for New Brunswick. Canada. Wetlands 27 (4), 846–854. https://doi.org/10.1672/0277-5212(2007)27[846:MWACOT]2.0.CO;2.

Murphy, P.N.C., Ogilvie, J., Meng, F.R., White, B., Bhatti, J.S., Arp, P.A., 2011. Modelling and mapping topographic variations in forest soils at high resolution: A case study. Ecol. Model. 222 (14), 2314–2332. https://doi.org/10.1016/j.ecolmodel.2011.01.003.

Nielsen, D., 2016. Tree Boosting With XGBoost - Why Does XGBoost Win "Every" Machine Learning Competition? Master Thesis, Norwegian University of Science and Technology, Trondheim, 98 pp.

Nussbaum, M., Spiess, K., Baltensweiler, A., Grob, U., Keller, A., Greiner, L., Schaepman, M.E., Papritz, A., 2018. Evaluation of digital soil mapping approaches with large sets of environmental covariates. Soil (Germany) 4 (1), 1–22. https://doi.org/10.5194/soil-4-1-2018.

Nyberg, L., Rodhe, A., Bishop, K., 1999. Water transit times and flow paths from two line injections of ^{3}H and ^{36}Cl in a microcatchment at Gårdsjon. Sweden. Hydrol. Process. 13 (11), 1557–1575. https://doi.org/10.1002/(SICI)1099-1085(19990815)13:11<1557::AID-HYP835>3.0.CO;2-S.

O'Neil, G.L., Goodall, J.L., Behl, M., Saby, L., 2020. Deep learning Using Physically-Informed Input Data for Wetland Identification. Environ. Modell. Softw. 126, 104665 https://doi.org/10.1016/j.envsoft.2020.104665.

Ploum, S.W., Leach, J.A., Kuglerová, L., Laudon, H., 2018. Thermal detection of discrete riparian inflow points (DRIPs) during contrasting hydrological events. Hydrol Process 32 (19), 3049–3050. https://doi.org/10.1002/hyp.13184.

Powers, D.M.W., 2011. Evaluation: from Precision, Recall and F-measure to ROC, Informedness, Markedness and Correlation. J. Mach. Learn. Technol. 2 (1), 37–63. https://doi.org/10.9735/2229-3981.

Quinn, P.F., Beven, K.J., 1993. Spatial and Temporal Predictions of Soil-Moisture Dynamics, Runoff, Variable Source Areas and Evapotranspiration for Plynlimon. Mid-Wales. Hydrol Process 7 (4), 425–448. https://doi.org/10.1002/hyp.3360070407.

Rashmi, K.V., Gilad-Bachrach, R., 2015. DART: Dropouts meet Multiple Additive Regression Trees, 18th International Conference on Artificial Intelligence and Statistics (AISTATS). W&CP, San Diego, CA, USA, JMLR.

Rennó, C.D., Nobre, A.D., Cuartas, L.A., Soares, J.V., Hodnett, M.G., Tomasella, J., Waterloo, M.J., 2008. HAND, a new terrain descriptor using SRTM-DEM: Mapping terra-firme rainforest environments in Amazonia. Remote Sens. Environ. 112 (9), 3469–3481. https://doi.org/10.1016/j.rse.2008.03.018.

Ring, E., Ågren, A., Bergkvist, I., Finér, L., Johansson, F., Högbom, L., 2020. A guide to using wet area maps in forestry, Skogforsk arbetsrapport 1051-2020, Uppsala, 36 pp.

Ripley, B.D., 1996. Pattern Recognition and Neural Networks. Cambridge University Press, Cambridge. https://doi.org/10.1017/CBO9780511812651.

Sabaghy, S., Walker, J.P., Renzullo, L.J., Akbar, R., Chan, S., Chaubell, J., Das, N., Dunbar, R.S., Entekhabi, D., Gevaert, A., Jackson, T.J., Loew, A., Merlin, O., Moghaddam, M., Peng, J., Peng, J.Z., Piepmeier, J., Rudiger, C., Stefan, V., Wu, X.L., Ye, N., Yueh, S., 2020. Comprehensive analysis of alternative downscaled soil moisture products. Remote Sens. Environ. 239, 111586 https://doi.org/10.1016/j.rse.2019.111586.

Schöllin, M., Daher, K.B., 2019. Land use in Sweden, Seventh edition. Statistics Sweden, Örebro, p. 187.

Seneviratne, S.I., Corti, T., Davin, E.L., Hirschi, M., Jaeger, E.B., Lehner, I., Orlowsky, B., Teuling, A.J., 2010. Investigating soil moisture-climate interactions in a changing climate: A review. Earth. Sci. Rev. 99 (3–4), 125–161. https://doi.org/10.1016/j.earscirev.2010.02.004.

Sørensen, R., Seibert, J., 2007. Effects of DEM resolution on the calculation of topographical indices: TWI and its components. J. Hydrol. 347 (1–2), 79–89. https://doi.org/10.1016/j.jhydrol.2007.09.001.

Story, M., Congalton, R.G., 1986. Accuracy Assessment - a Users Perspective. Photogramm. Eng. Rem. S. 52 (3), 397–399.

Tenenbaum, D.E., Band, L.E., Kenworthy, S.T., Tague, C.L., 2006. Analysis of soil moisture patterns in forested and suburban catchments in Baltimore, Maryland, using high-resolution photogrammetric and LIDAR digital elevation datasets. Hydrol. Process. 20 (2), 219–240. https://doi.org/10.1002/hyp.5895.

Wei, L., Zhou, H., Link, T.E., Kavanagh, K.L., Hubbart, J.A., Du, E.H., Hudak, A.T., Marshall, J.D., 2018. Forest productivity varies with soil moisture more than temperature in a small montane watershed. Agr. Forest Meteorol. 259, 211–221. https://doi.org/10.1016/j.agrformet.2018.05.012.

White, B., Ogilvie, J., Campbell, D.M.H., Hiltz, D., Gauthier, B., Chisholm, H.K., Wen, H. K., Murphy, P.N.C., Arp, P.A., 2012. Using the Cartographic Depth-to-Water Index to Locate Small Streams and Associated Wet Areas across Landscapes. Can. Water Resour. J. 37 (4), 333–347. https://doi.org/10.4296/cwrj2011-909.

Zeng, L.L., Hu, S., Xiang, D.X., Zhang, X., Li, D.R., Li, L., Zhang, T.Q., 2019. Multilayer Soil Moisture Mapping at a Regional Scale from Multisource Data via a Machine Learning Method. Remote Sens. 11 (3), 284. https://doi.org/10.3390/rs11030284.